


Atomistic molecular dynamics simulations on the interaction of TEMPO-oxidized cellulose nanofibrils in water

Antti Paajanen  · Yogesh Sonavane · Dominika Ignasiak · Jukka A. Ketoja · Thaddeus Maloney · Sami Paavilainen

Received: 1 July 2016 / Accepted: 23 September 2016 / Published online: 28 September 2016
© Springer Science+Business Media Dordrecht 2016

Abstract Atomistic molecular dynamics simulations were carried out to obtain information on the rheological, aggregation and disintegration properties of carboxylated (TEMPO-oxidized) cellulose nanofibrils with different functionalization levels. The magnitude of the inter-fibril interaction was quantified for parallel nanofibrils using the umbrella sampling method. The obtained potential of mean force was found highly sensitive to the charge configuration for intermediate functionalization levels. This feature was further studied with an electrostatic model for similar charge configurations and system periodicity as in the case of the molecular dynamics simulations. The electrostatic contribution of the charged surfaces varied from repulsive to attractive depending on the distribution of the carboxylate groups and nearby counter-ions, as well as the distance between the fibrils. The simulated deviations from average behavior for single fibrils in both models suggest heterogeneity in their aggregation and disintegration

behavior. This was seen in disintegration experiments, where the differences in disintegration energy and in the structural variation qualitatively agreed with the model predictions. As to aggregation behavior, the studied case with parallel fibrils reflects the upper boundary of the repulsive interaction.

Keywords Cellulose nanofibril · Functionalization · TEMPO-oxidation · Molecular dynamics · Electrostatic interaction

Introduction

Cellulose is found in nature in hierarchical structures starting from nanofibrils (also called elementary fibrils, diameter 3.5–7.1 nm depending on the origin), their clusters called cellulose nanofibers (diameter about 20 nm), macrofibrils and the actual fibers (Chinga-Carrasco 2011). Novel processing methods enable one to disintegrate cellulosic fiber materials to the micro and nanometre scale (Postek et al. 2013). The disintegrated materials are often referred to as micro or nanofibrillated cellulose (MFC and NFC, respectively). Recently, NFC consisting mainly of cellulose nanofibers has attracted a lot of attention from the scientific community due to its unique features and the potential for use in sustainable applications (Paster et al. 2003; Moon et al. 2011). The abundance and renewability of cellulose makes

A. Paajanen (✉) · J. A. Ketoja
VTT Technical Research Centre of Finland Ltd.,
P.O. Box 1000, 02044 VTT, Espoo, Finland
e-mail: antti.paajanen@vtt.fi

Y. Sonavane · T. Maloney
Department of Forest Products Technology, Aalto
University, P.O. Box 11000, 00076 Aalto, Espoo, Finland

D. Ignasiak · S. Paavilainen
Department of Physics, Tampere University of
Technology, P.O. Box 692, 33101 Tampere, Finland

NFC available from a number of sources including wood, cotton, sugar beet and other plant-based, as well as animal-origin materials. NFC can be used as a raw material for lightweight, biodegradable and thus environmentally friendly products, which have desirable mechanical properties such as high strength and stiffness. These key characteristics make NFC a promising material for a number of applications in the fields of paper and cardboard industry, medical devices and many other fields, with applications ranging from body armor to filtration systems and water desalination technologies (Moon et al. 2011), and use in the diaper industry as a superabsorbent material (Brodin et al. 2013a, b).

Unfortunately, the large physical size and strong structure of biomass makes size-reduction very energy intensive. Various mechanical (Brodin et al. 2013b; Herrick et al. 1983; Turbak et al. 1983), chemical (Saito et al. 2006, Wågberg et al. 2008) and enzymatic (Pääkkö et al. 2007; Henriksson et al. 2007) pre-treatments have been suggested to reduce the disintegration energy in the production of MFC and NFC. The oxidative treatment of native cellulose by Saito et al. (2006) is an approach which allows the introduction of negatively charged carboxylate groups on the surface of cellulose fibers. The oxidation reaction, which is catalyzed by 2,2,6,6-tetramethylpiperidine 1-oxyl (TEMPO) radicals, and followed by a mechanical treatment, allows preparation of cellulose nanofiber suspensions at room temperature and alkaline pH (Saito and Isogai 2005; Saito et al. 2006, 2007, 2009). In this process, oxidation is used as a pre-treatment step. After removing the spent oxidation chemicals with a displacement washing step, the pulp is disintegrated, thus forming nanofibrillar cellulose (NFC).

The presence of charged surface groups does not affect only the disintegration properties, but also the aggregation and rheological properties in suspensions. Fall et al. (2011) studied the colloidal stability of aqueous NFC dispersions. They used a model to describe deprotonation and electrostatic screening which enabled the calculation of fibril–fibril electric interaction potential at a given pH and ionic strength. By including the interactions of the ions with (deprotonated) carboxyl groups, the predicted surface potential compared qualitatively well with the value of the zeta potential obtained from electrophoretic mobility measurements. The model was further compared with DLVO theory where the total interaction energy came

from the sum of van der Waals interaction energy and the energy due to the overlap of the electric double layers. Fukuzumi et al. (2014) studied further the dispersion stability of TEMPO-oxidized cellulose nanofibrils in water as a function of salt addition. The stability of the fibril dispersions was evaluated based on their light transmittances, viscosities and weight fractions of aggregated gel. The dispersions were stable up to 50 mM NaCl. However, a significant amount of aggregated gel particles was observed at 100 mM NaCl and higher concentrations. The shear viscosity increased up to the 100 mM concentration level but then decreased at higher concentrations due to phase separation of the gel particles and the supernatant. These results were analyzed with similar DLVO model as the one used by Fall et al. (2011) so that both parallel and perpendicular alignments of the fibrils were considered. When the maximum potential energy was lower than $k_B T$, the aggregation of the fibrils by Brownian motion became possible. This took place at lower concentration for the perpendicular alignment (around 100 mM NaCl) than for the parallel alignment (around 200–400 mM NaCl).

The present work takes the modelling effort beyond the earlier continuous descriptions by introducing an atomistic molecular dynamics (MD) simulation approach to study the effect of charged functional groups on the inter-fibril interaction. MD simulations have previously found extensive use in the study of the properties of cellulose. This includes studies on the crystal structure and elasticity (Matthews et al. 2006; Eichhorn and Davies 2006; Matthews et al. 2011; Zhang et al. 2011; Paavilainen et al. 2011), swelling behavior (Yui et al. 2006, 2007), mechanical properties of nanofibrils (Paavilainen et al. 2012), and enzymatic disintegration of NFC (Orlowski et al. 2015). Moreover, in their recent work, Oehme et al. (2015) used MD simulations to study the adsorption of cellulose nanofibrils onto one another. In this article, a similar approach is used to investigate the interactions between fibrils with incorporated surface carboxylate groups. The results are then compared with the predictions of an electrostatic model to further investigate the role of Coulomb and short range forces. The modelling is complemented with experiments to evaluate the energy required to disintegrate pulp to form the fibrils. The observed heterogeneity shown in the electric interactions of the models is then reflected against the experimental results.

Methods

Experimental

The raw material for the NFC production was never-dried bleached Scandinavian softwood kraft pulp. The chemical treatments were carried out with TEMPO (Sigma-Aldrich, 98 % purity), sodium bromide (NaBr, Scharlau, 99.5 % reagent grade), sodium hydroxide (NaOH, Scharlau, 99 % reagent grade), hydrochloric acid (HCl, Scharlau, solution 1 M reagent grade), and sodium hypochlorite (NaClO, Scharlau, solution 15 % w/v extra pure). Deionized water was used throughout the process. The details of the process steps are given by Brodin et al. (2013b) and only the main features are summarized here.

The oxidation experiments were performed in a cylindrical glass vessel (volume of 25 litres) with a regulated stirrer assembly. The vessel was surrounded by a water bath with automatically regulated temperature. Cellulose fibers in the form of pulp suspension in water were subjected to various oxidation and temperature levels. During the TEMPO oxidation reaction, both (a) the reaction temperature (around 30 and 50 °C), and (b) the concentration of sodium hypochlorite (2.5, 3.0 and 5.0 mmol NaClO/g pulp) were varied. Note that only the reaction temperature was varied, and the temperature during the grinding was not measured. The concentration of hypochlorite ions was determined by iodometric titration prior to the oxidation experiments.

Each chemical batch included pulp, TEMPO, NaBr and deionized water. Before the oxidation was started, the pulp suspension was heated up to the target temperature. The reaction was initiated by the addition of the oxidant (NaClO), and the pH was kept at 10.0 throughout the reaction by using a Ph-stat with automatic addition of 2 M sodium hydroxide solution. Manual addition of 2 M sodium hydroxide was made in the early phase of the reaction due to the limited capacity of the pH-stat. The reaction system was maintained at 2 % pulp consistency and the suspension was continuously stirred during the reaction. Completion of the oxidation reaction was achieved when the pH of the reaction liquid did not increase any longer, despite an excess amount of sodium hydroxide.

The washing step separated pulp from the reaction liquid after chemical treatment with the help of filtration. Each washing step was done with plenty of

deionized water. At the end of the washing cycle, the pulp was dewatered to about 16–20 % consistency and stored at 4 °C in a cooling room.

An Ystral Z 80-3 dispersion unit from Ystral GmbH, Germany, was used in the disintegration process. The washed pulp was used to prepare a suspension of 2 % consistency before disintegration. In the Ystral system, the amount of used electric energy for each disintegration pass could be read directly from an external digital panel. Thus, the power consumption for every pass could be recorded for the given rotational speed (3000 or 5000 rpm). First, the electrical energy input for an empty run was measured. For the actual disintegration experiments, the specific time needed for disintegration was obtained by carefully monitoring the flow rate at the outlet. The total energy demand E_{tot} was then calculated as:

$$E_{\text{tot}} = \frac{1}{m} \sum_{\text{passes}} \frac{P - P_0}{t} \quad (1)$$

where P_0 is the power consumption in an empty run and P is the power consumption in a loaded run, t is time and m is the mass of pulp in the slurry. The (length-weighted) average fiber length after disintegration was measured with a Metso Kajaani FS-300 fiber analyzer, and results were reported according to the TAPPI T271 standard. The fiber length analysis was done with respect to extent of disintegration at various oxidation and input energy levels. The sample was diluted with water and dispersed well before the measurement.

The disintegration was also studied using a high-pressure homogenizer (Microfluidics M-110P), where the process steps were similar including the TEMPO-oxidation reaction, washing with water and filtering. The process temperatures were 20, 30 and 50 °C and the functionalization levels were 2.5, 3.0 and 5.0 mmol NaClO/g pulp. The disintegration of the pulp with increasing number of passes in the homogenizer was performed until 10 passes was reached. The obtained NFC samples were stored at 4 °C and later analyzed by atomic-force microscopy (AFM).

Molecular dynamics model for fibril interaction

All-atom MD simulations were used to quantify the interactions between parallel, surface carboxylated,

cellulose nanofibrils in water. A periodic model system was constructed starting from the functionalization of a single nanofibril, and leading to a series of umbrella sampling simulations for determining the potential of mean force (PMF) for separating such fibrils. The MD simulations were performed using the GROMACS software package (Pronk et al. 2013) with the OPLS-AA all-atom force field (Jorgensen et al. 1996) as the interaction model.

The starting point, an atomistic model of a cellulose nanofibril, was obtained from Paavilainen et al. (2011), originally constructed on the basis of crystallographic unit cell data given in (Nishiyama et al. 2002). The model fibril consists of 36 cellulose molecules (Ding et al. 2014), each 20 glucose residues long, together forming a rectangular hexahedral shape with the dimensions $(3.6 \times 3.5 \times 10.5) \text{ nm}^3$. The length of the model fibril is smaller than the average length of crystalline regions in wood fibrils (Andersson et al. 2003). The cellulose is in the I β structure, with hydrogen bonding corresponding to the network A structure proposed in (Nishiyama et al. 2008).

The basic model was modified to represent a fibril with incorporated surface carboxylate groups (Fig. 1). This was achieved by randomly substituting hydroxymethyl groups with carboxylate groups on the fibril surface. Every second hydroxymethyl group of each surface chain is available for substitution, giving a maximum of 200 carboxylate groups on the surface of a functionalized fibril. Model fibrils with 0, 50, 100, 150 and 200 carboxylate groups were created for studying the whole range of possible functionalization

levels. Moreover, five realizations with distinct carboxylate group distributions were created for each functionalization level. The modification scheme is supported by experimental findings both with regard the reaction sites (Saito et al. 2009; Saito and Isogai 2004) and their availability (Saito et al. 2007).

The MD simulation set-up for quantifying inter-fibril interactions was constructed in the following manner for each combination of functionalization level and carboxylate group distribution. The model fibril and its duplicate copy were embedded in a periodic simulation domain of $(13.0 \times 6.5 \times 14.0) \text{ nm}^3$, aligned parallel and roughly 3 nm apart from each other (surface-to-surface distance). Potential energy minimization was then performed to correct for unnaturally large forces imposed by the added carboxylate groups. The rest of the simulation domain was filled with water molecules, yielding a system with a density of 1.2 g/cm^3 . Sodium and chloride ions were added to produce a neutral solution with a typical salt concentration of 250 mM. The electrostatic screening by added salt (Fall et al. 2011; Fukuzumi et al. 2014) was described by adding sodium ions close to the carboxylate groups so that the overall charge was locally neutralized (see Fig. 1). After the solvation, a potential energy minimization was again performed. The system was then equilibrated in a 1 ps MD simulation in the isothermal-isobaric (NPT) ensemble, at absolute zero temperature and 1 bar pressure.

The umbrella sampling method (Torrie and Valleau 1977; Kästner 2011) and the weighted histogram

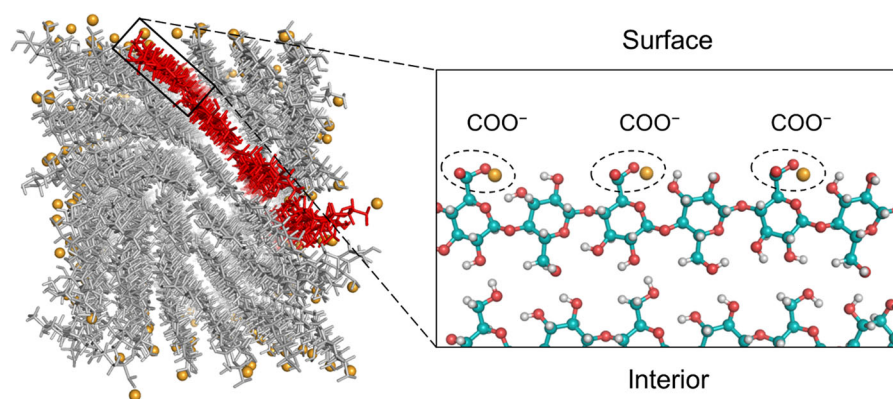


Fig. 1 Atomistic model of a carboxylated cellulose nanofibril. On the left: view along the fibril's longitudinal axis with nearby sodium ions visible; color legend: *gray* (carbon, oxygen and

hydrogen), *orange* (sodium), *red* (highlight). On the right: carboxylate groups and sodium ions on the fibril surface; color legend: *cyan* (carbon), *red* (oxygen), *light gray* (hydrogen)

analysis method (WHAM) (Kumar et al. 1992) were used to evaluate the interaction magnitude as a function of the inter-fibril distance. In the umbrella sampling method, a harmonic biasing potential is added to the force calculation to improve sampling along the chosen reaction coordinate. WHAM is used to calculate the PMF as a function of the reaction coordinate from a series of umbrella sampling simulations. The PMF is, by definition, the potential that reproduces the mean force observed in the simulations. In this study, the chosen reaction coordinate was the inter-fibril distance in a situation where the fibrils are separated (or brought together) maintaining the parallel orientation. A visual summary of the umbrella sampling procedure is given in Fig. 2.

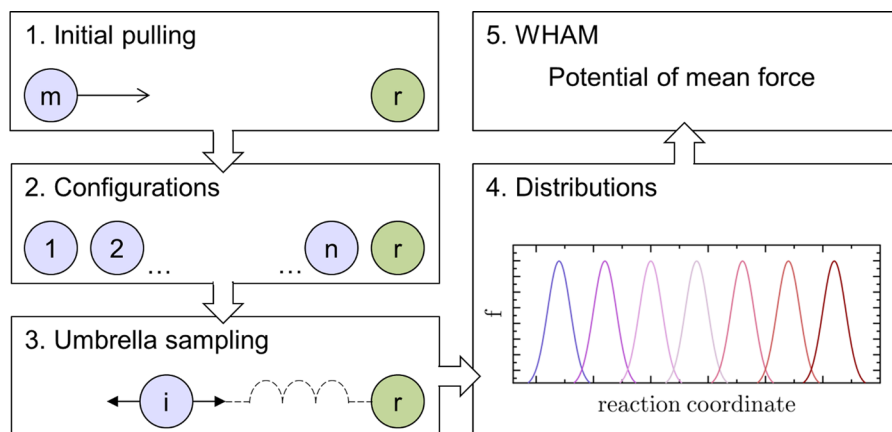
The procedure began with an initial pulling simulation, where one of the fibrils (the reference fibril) was kept fixed by restraining one of its innermost chains, while the other fibril (the mobile fibril) was pulled towards it at a constant rate of 0.01 nm/ps, for a total distance of 2.7 nm. The pulling simulations were performed in the canonical (NVT) ensemble at a temperature of 350 K, with a total simulation time of 270 ps. The system configuration was stored at 0.1 nm intervals.

The stored system configurations were used to create a series of umbrella sampling simulations. Each configuration would correspond to a different position along the reaction coordinate, measured as the centre-of-mass (COM) distance between the fibrils. Two versions of the biasing potential were implemented: (1) 1D, applied only along the direction of the reaction coordinate (i.e. the x-coordinate of the simulation domain), and (2) 2D, applied along the direction of the

reaction coordinate and along the direction of the fibrils' longitudinal axes (i.e. both x- and z-coordinates of the simulation domain). In both cases, the force constant of the added harmonic potential was 4000 kJ/(mol·nm). The simulations were performed in the canonical ensemble at a temperature of 350 K. Sampling times between 1 and 8 ns were used. WHAM, as implemented in the GROMACS analysis programme `g_wham` (Hub et al. 2010), was used to calculate the PMF curves. The GROMACS utility `g_hbond` was used to monitor the formation of inter-fibril hydrogen bonds, and the utilities `g_dist` and `g_rotmat` were used to monitor fluctuations in the inter-fibril COM-distance and the orientations of the fibrils during the course of the sampling simulations.

The MD simulations were performed using GROMACS 4.6.4, together with the OPLS-AA all-atom force field extended for carbohydrates. OPLS-AA considers both the bond lengths and the bond and torsional angles in calculating the bonded interactions. The LINCS bond constraint method (Hess et al. 1997) was used to preserve constant length for all covalent bonds. No bond-angle constraints were used. OPLS-AA calculates the non-bonded terms using the Lennard-Jones (cut-off) potential for the van der Waals interactions, and the Coulomb potential for the electrostatic interactions. The van der Waals interaction cut-off was set to 1 nm. For the long range electrostatic interactions, the particle-mesh Ewald (PME) method (Essmann et al. 1995), with 1 nm cut-off range, was used. The TIP3P three-site model was used to describe water. The velocity-rescaled Berendsen thermostat (Bussi et al. 2007) was used for temperature control with a time constant of 0.1 ps, and

Fig. 2 Visual summary of the umbrella sampling method. The *green circle* represents the reference fibril and the *blue circles* represent the mobile fibril at different positions along the reaction coordinate



the Berendsen semi-isotropic barostat was used for pressure coupling with a time constant of 1 ps. Integration of the equations of motion was performed using the leap-frog algorithm with a constant time step of 2 fs, except in the equilibration simulations, where a 1 fs time step was used. Neighbor list update was performed at an interval of 50 time steps. The steepest descent method was used for the potential energy minimizations.

Electrostatic model for fibril interaction

Long-range electrostatic forces are expected to dominate the fibril–fibril interaction at distances larger than 1 nm. Moreover, the electrostatic force associated with the periodic images of the simulation domain can also have a significant effect on the system. Therefore, it is helpful to consider these factors with a simplified model for the electrostatic interactions only.

An idealized model was created to study the contribution of the carboxylate groups and the adjacent sodium counter-ions to the overall interaction. The sodium ions present in water tend to screen the negative carboxylate groups on the fibril surface. In the model, single point particles with negative and positive elementary charge were used to represent the carboxylate groups and the sodium ions, respectively. The oppositely charged particles were distributed in pairs among 200 lattice sites, approximating the possible locations of carboxylate groups on the surface of the cellulose nanofibril (Fig. 3). The model fibril and its duplicate copy were situated in a simulation domain of $(13.0 \times 6.5 \times 14.0) \text{ nm}^3$, mirroring the MD set-up both with regard the fibril size and the

overall geometry. The inter-fibril distance was varied by keeping one of the fibrils fixed (the reference fibril) while moving the other (the mobile fibril) in the direction of the x-coordinate.

The electric potential of the reference fibril due to the electric field of the mobile fibril was determined for each inter-fibril distance:

$$V = \sum_{i=1}^N \sum_{j=1}^N \frac{1}{4\pi\epsilon_0} \frac{q_j^{(2)}}{|r_i^{(1)} - r_j^{(2)}|} \quad (2)$$

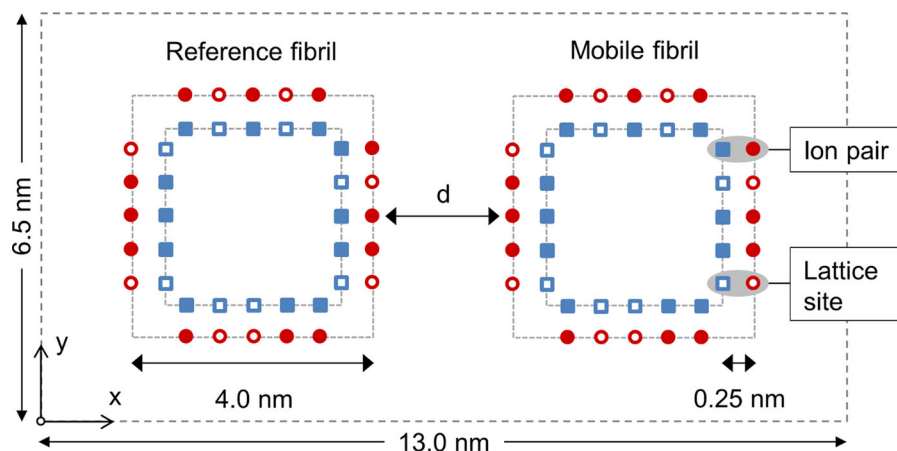
where N is the number of charged particles in the model fibril, $r_i^{(j)}$ is the coordinate vector and $q_i^{(j)}$ is the charge of the i^{th} particle of fibril j , and ϵ_0 is the vacuum permittivity. Surface-to-surface distances between 0.5 and 3.25 nm were considered. The electric potential for each intermediate functionalization level was determined by averaging over 100 random charge group configurations. Both an isolated system, and a system with periodic boundary conditions were considered.

Results and discussion

Disintegration experiments

The interactions between functionalized fibrils affect the clustering of these fibrils to form larger cellulosic structures of the wood fiber wall. Thus, the fibril–fibril interaction can be expected to be relevant not only for colloidal stability but also for the disintegration process itself. For most of the previous works, mechanical degradation has been measured as passes

Fig. 3 The electrostatic interaction model viewed along the direction of the fibrils' longitudinal axis. Positively and negatively charged ions are shown as *solid red and blue dots* respectively. Vacant lattice sites are shown as *circles with a white centre*. The *outer dashed line* indicates the boundaries of the periodic domain



in the homogenizer or grinder, and the actual energy demand during mechanical degradation has not been reported. This is still a crucial economical factor in the production of MFC.

The energy needed to disintegrate cellulose fibers is shown in Fig. 4 for 5000 rpm (the qualitative behavior was similar for 3000 rpm). Both the reaction temperature and functionalization level affected the energy and the degree of disintegration as indicated by the average fiber length. With 5.0 mmol/g functionalization, a couple of passes were sufficient to disintegrate most of the pulp, whereas a similar disintegration degree was not achieved even with eight passes at the 2.5 mmol/g functionalization level.

Qualitatively similar findings were obtained by studying disintegration in a high pressure homogenizer for the same functionalization process. The heterogeneity of the disintegrated structure at the low level of functionalization could be seen in the AFM images taken from the formed NFC after ten passes (see Fig. 5). The NFC quality appears finer at 5.0 mmol/g than at 2.5 mmol/g, and the overall structure appears more homogeneous at the higher level of functionalization. The structural features could be affected both by the fibril disintegration and their aggregation when forming the AFM sample.

The observed reduction in the required disintegration energy (Fig. 4) and better homogeneity of NFC with increasing concentration of sodium hypochlorite (Fig. 5) could be explained by similar repulsive forces between the fibrils as in the case of colloidal systems

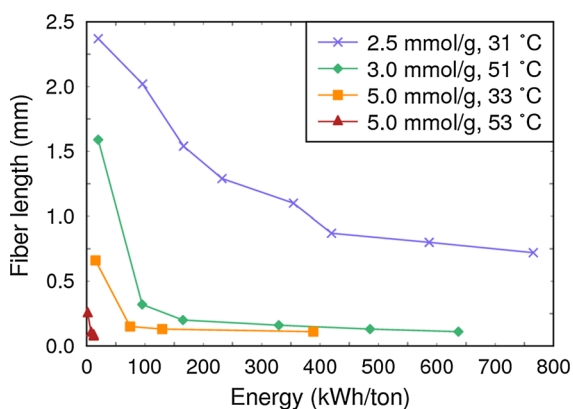


Fig. 4 Experimental grinding energy at different levels of functionalization and reaction temperature for 5000 rpm. The degree of disintegration is indirectly indicated by the average fiber length. The temperatures refer to reaction temperatures

(Fall et al. 2011; Fukuzumi et al. 2014). Modelling the effect of the charges on fibril interactions helps in understanding the mechanisms underlying these experimental results.

Molecular dynamics simulations

The two fibrils interact with one another in a complex way because of several reasons. Firstly, the non-contacting parallel alignment is unstable, which easily leads to a drift in fibril positions at short distances. This has been also seen in recent experiments for non-functionalized cellulose nanocrystals (Schütz et al. 2015). Secondly, the interaction is sensitive to the charge group distributions, which leads to deviations in the simulated forces. Thirdly, the movement of water molecules and sodium ions in the solvent contribute to the overall interaction. These complexities are expected to take place in real experimental systems as well. Therefore, in below we will discuss not only the averaged interaction strength but also qualitative and quantitative features of single fibril–fibril interactions that may drive the heterogeneity of the system behavior.

Figure 6 shows an example of an initial pulling simulation (step 1 in Fig. 2) where the mobile fibril is drawn close the reference fibril with constant velocity. The movement is fairly stable until about 3.7 nm COM-distance (Fig. 6b) (corresponding to less than 1 nm in surface-to-surface distance) when hydrogen bonds begin to form between the fibrils (Fig. 7) and the parallel face-to-face alignment is lost.

In the umbrella sampling simulations with longer simulation times, both drifts in the yz -plane and significant tilting of the moving fibril could be observed, the specific dynamics varying from case to case. The uneven distribution of the surface charge groups is a probable cause for the differences in behavior between individual simulations. The instability can be further affected by the presence and dynamic exchange of sodium ions in the water phase between the fibrils (see Figs. 8, 9). These ions screen the surface charge groups and thus reduce the repulsive interaction between the fibrils. This could stabilize the interaction at large distances. However, when the fibrils come very close to one another, the small movement of the sodium ions around the surface charge groups probably comes relevant. This movement was analyzed with radial distribution functions

Fig. 5 AFM images of NFC at **a** 5.0 mmol/g and **c** 2.5 mmol/g functionalization level and 50 °C temperature after ten passes in a homogenizer. Figures **b** 5.0 mmol/g, and **d** 2.5 mmol/g, show the structural edges of the AFM images. The structural distribution appears more even and finer for the higher functionalization level

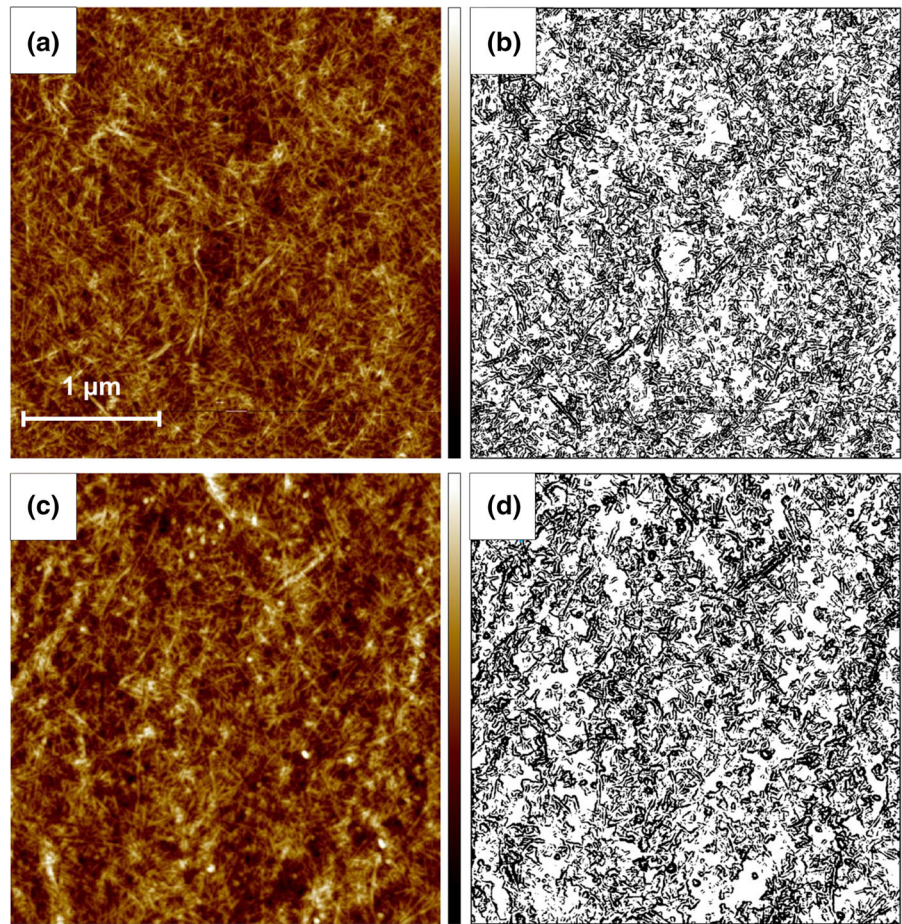
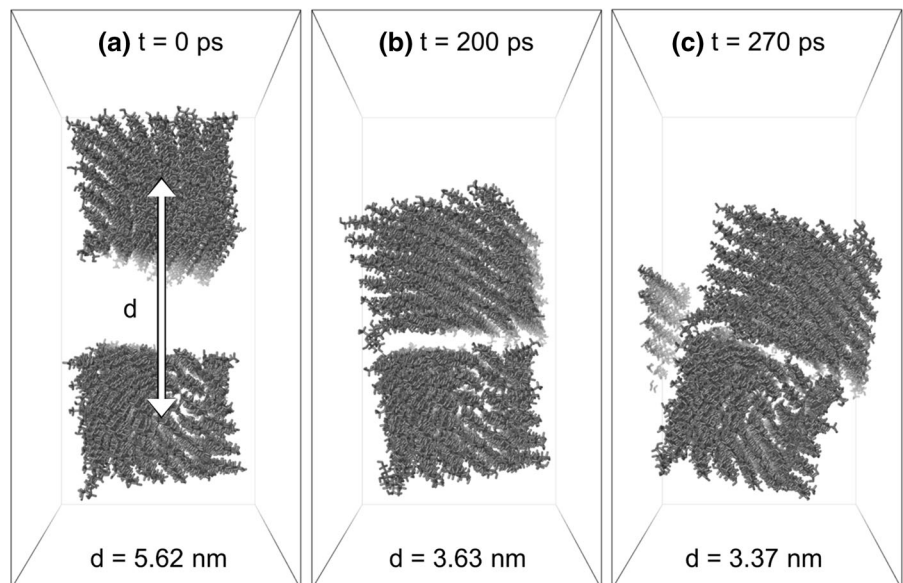


Fig. 6 Typical fibril behavior in the initial pulling simulations: **a** parallel alignment in the beginning, **b** alignment maintained until hydrogen bonds begin to form, **c** alignment lost due to further pulling along the initial direction. The water molecules are hidden for improved clarity



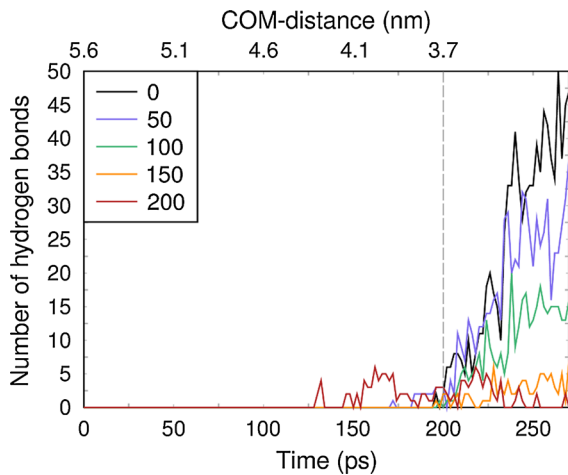
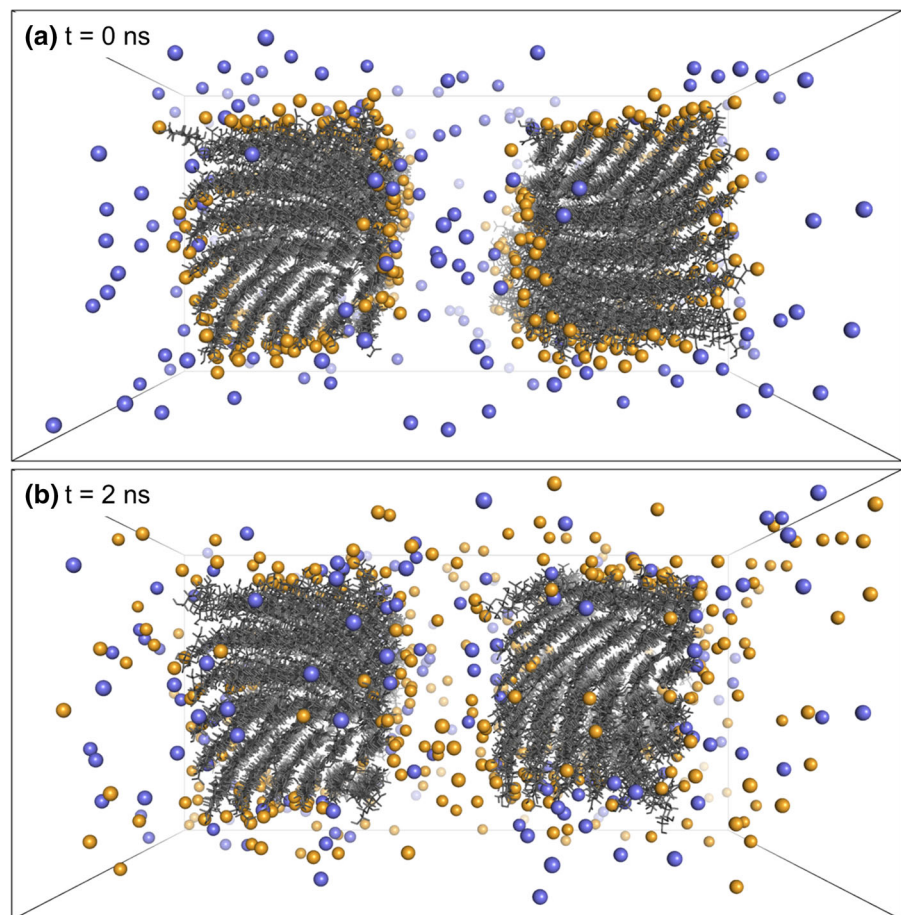


Fig. 7 Number of inter-fibril hydrogen bonds during the initial pulling simulations. The *five* curves correspond to the different functionalization levels. System configurations from the first 200 ps were used in the umbrella sampling simulations

Fig. 8 Distribution of sodium ions in the water surrounding the fibrils in the fully modified (200) case and largest inter-fibril distance: **a** ions initially at the fibril surfaces are shown in *orange*, whereas the ions initially in bulk water are shown in *blue*; **b** ion exchange from fibril surface to water and vice versa is seen after the 2 ns simulation period. The water molecules are hidden for improved clarity



(RDF). RDFs obtained from the 2 ns sampling simulations of the functionalization case 200 are shown in (Fig. 9). The RDF for carboxylate-sodium coupling has a first contact maximum at 0.23 nm, and a second maximum at 0.43 nm. This structure is retained during the simulation despite dynamic charge exchange taking place between the fibril surfaces and bulk water. Considering all sodium ions in the system, the RDFs became steady after about 250 ps simulation time, i.e. relatively quickly compared to the total sampling times.

PMF curves obtained from the umbrella sampling analyses were used to visualize the interaction between the fibrils. The PMF curves for the different functionalization levels are shown in Fig. 10. A large variation in PMF as a function of fibril separation corresponds to a significant average repulsion between the fibrils. In practice, this could mean reduced

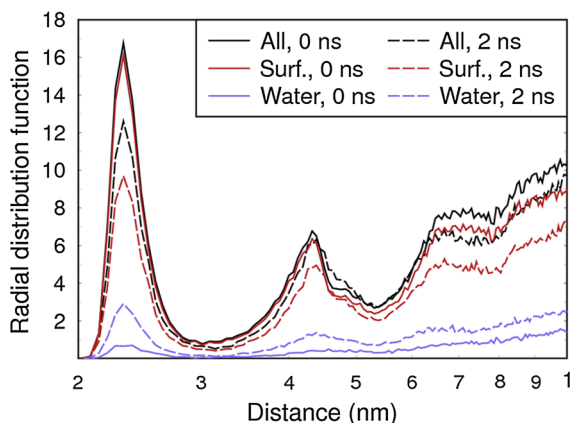


Fig. 9 Average radial distribution functions for the carboxylate-sodium distance, calculated from the five parallel realizations of the functionalization case 200 with the largest inter-fibril separation. *Solid lines* represent the situation at 0 ns and *dashed lines* at 2 ns of simulated time. Color legend: *black* (all sodium ions), *red* (sodium ions initially at the surfaces), *blue* (sodium ions initially in the water)

disintegration energy or a more stable colloidal system. The tendency of the free fibril to deviate from the parallel alignment (including both COM-distance drifting and rotations around the COM) during the sampling simulations caused significant effects in the PMF levels. For 8 ns sampling time and the umbrella potential in the x-direction only, such deviations took always place. Adding the z-dimension to the umbrella potential resulted in less drifting, but the deviation was often big enough to make the PMF results suspicious. Both COM-drifting and rotations around the COM could be minimized by reducing the sampling time from 8 to 1 ns (see Fig. 10a). This worked even without the added z-potential. However, reducing the sampling time increased noise in the PMF curves. An intermediate solution was to use 2 ns sampling time with the umbrella potential in both x- and z-directions (Fig. 10b). The increased sampling time reduced PMF noise significantly. There was still some drifting in both the COM-distance and the orientation of the free fibril, but these were considered to be at an acceptable level.

The average PMF curves generally follow the order of functionalization level, even if the scatter in PMF for the intermediate levels is rather large (see Fig. 11). In fact, this scatter is of the same order of magnitude as the average PMF separation for the different functionalization levels. The repulsive interaction begins to increase significantly when the separation between

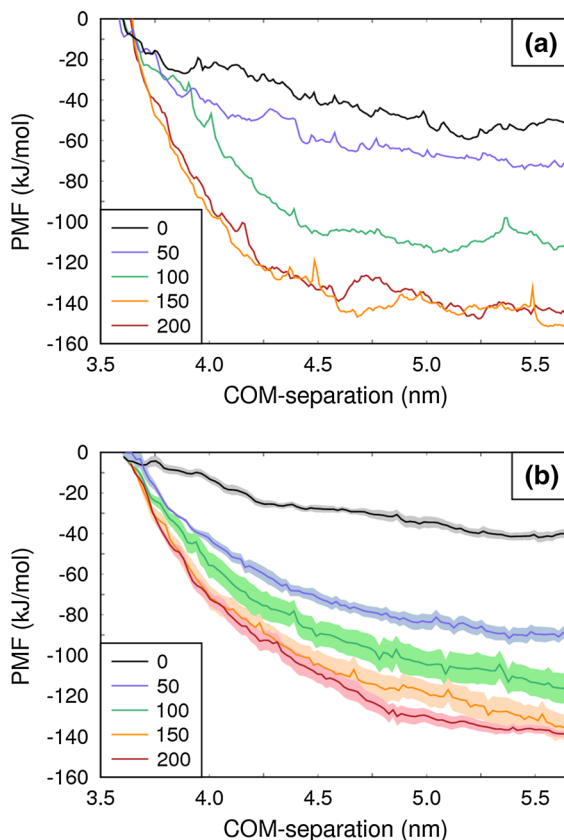


Fig. 10 PMF curves for separating the carboxylated cellulose nanofibrils: **a** 1 ns sampling with umbrella potential in the x-direction, **b** 2 ns sampling with umbrella potential in the x- and z-directions. In **b**, the curves are averaged over five realizations of the charge group distribution. *Solid colors* indicate the standard error of the mean. Note that possible attraction at distances shorter than 3.7 nm is not shown here

interacting fibril surfaces becomes smaller than 1 nm (COM-distances below 4 nm). For the unmodified fibrils the repulsive interaction is rather small and also a small attractive potential well is visible at COM-distance of 3.7 nm. At this distance there is no significant hydrogen bonding between the fibrils, so this weak potential well is caused by the water molecules binding the fibrils together. Pushing the fibrils even more together is restrained by the water layer in between the fibrils similarly to results found for the un-relaxed non-functionalized fibrils with the 3D-RISM-KH model (Stoyanov et al. 2014).

One should notice that the range of umbrella sampling simulations did not include COM-distances lower than 3.7 nm where inter-fibril hydrogen

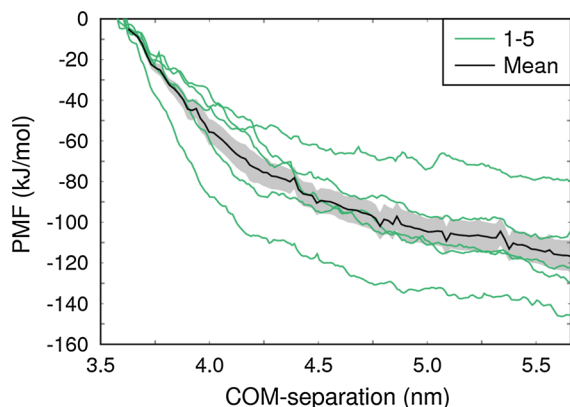


Fig. 11 PMF curves for the five realizations of the functionalization case 100. The mean and the standard error of the mean are indicated by the *black line* and the *light gray fill*, respectively

bonding would begin to take place (as shown in Fig. 7). In the initial pulling simulations fibrils were pushed towards each other also at these shorter distances to enable the fibrils to integrate. However, pushing also caused the fibrils to rotate around each other in a manner that was not repeatable between the different simulations. The number of hydrogen bonds was also very dependent on the angle between the fibrils and how the twists of the fibrils were adjusted to each other. Thus, the short-range forces were omitted from the umbrella sampling simulations and the PMF analysis shown in Fig. 10.

The simulated PMF can be compared with the disintegration energy of modified cellulose fibrils obtained experimentally. The fact that the experimental energy is affected by the charge of the carboxylate groups suggests that these charges are not limited to the fiber surfaces only, but they have access to the inner elementary fibrils of the fiber wall via diffusion. However, it is difficult to estimate how completely occupied the active sites are in the experimental case. Thus, only a qualitative comparison can be made. The observed decrease in the disintegration energy with the level of functionalization (Fig. 4) is similar to the behavior of the PMF. However, in the experiment the effect of functionalization seems to be even stronger than for the PMF. The screening caused by the moving counter ions reduces the simulated PMF, but this effect is expected to take place in the experimental system as well. A more exact quantitative analysis would require an estimate of the number of active sites in the experimental system. Moreover, the artificial finite-

size effects (due to the use of periodic boundary conditions) should be removed from the atomistic model. In the next section, this effect and the scatter observed in Figs. 10 and 11 for the different charge distributions is studied further with the help of the electrostatic model.

Electrostatic model

The variation in the interaction strength due to different charge group distributions is demonstrated in Fig. 12 using the electrostatic model. The scatter between individual realizations is larger than the average repulsive interaction between the fibrils. Surprisingly, some of the interactions are even attractive. These probably result from charge group distributions that match some of the positive ions of one fibril with the negative ions of the other. In any case,

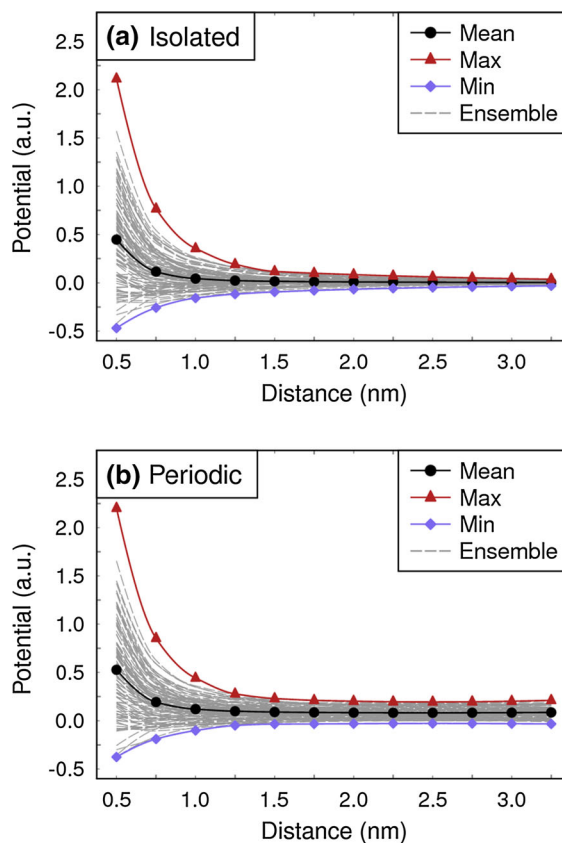


Fig. 12 The effect of surface charge distribution on the inter-fibril potential (arbitrary units) according to the electrostatic model: **a** isolated, and **b** periodic system. The *curves* correspond to the functionalization case 50

the figure suggests highly heterogeneous aggregation behavior in real experimental systems.

When averaging over 100 random charge group configurations for each functionalization level, the interaction potentials follow nicely the order of functionalization, as shown in Fig. 13. In all cases, the repulsive interaction begins to increase strongly when the separation of the fibril surfaces becomes less than 1 nm. This confirms the electrostatic origin of the similar behavior observed in the molecular dynamics simulations. The effect of periodic boundaries on the interaction can be seen by comparing Fig. 12a, b, as well as Fig. 13a, b. The periodic boundary condition is found to increase the separation between the potential curves, but this effect is smaller than the one coming from the direct inter-fibril interaction. A similar effect is expected to be present in the MD simulations.

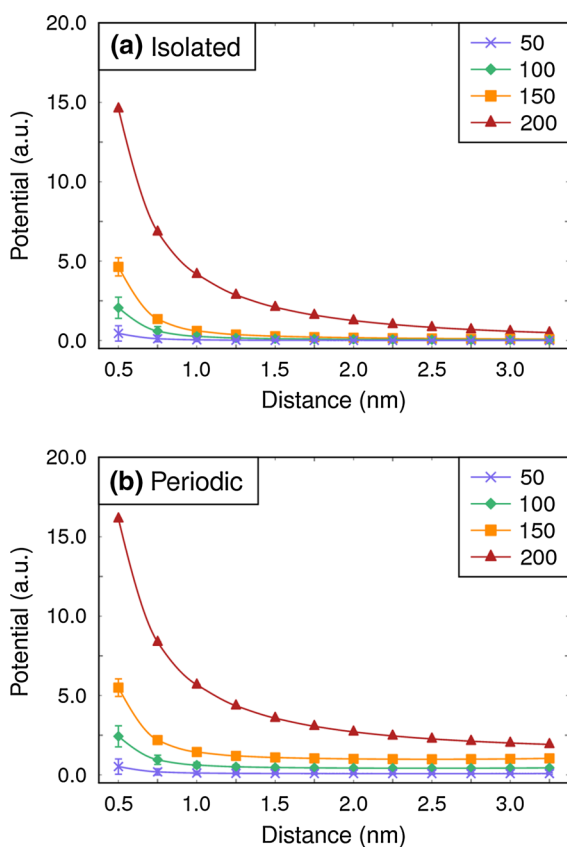


Fig. 13 The effect of net surface charge on the average inter-fibril potential (arbitrary units) according to the electrostatic model: **a** isolated, and **b** periodic system. The *error bars* indicate the standard error of the mean for 100 simulations

Conclusions

Molecular dynamics simulation appears to be a suitable method to study the properties of functionalized nanocellulose. The PMF calculation, even if approximate, can serve to evaluate the magnitude and variation of fibril repulsion for different levels of functionalization. The scatter of calculated inter-fibril interaction energies for TEMPO-oxidized nanofibrils was very large at intermediate functionalization levels. Our electrostatic interaction model indicated that the main cause of the scatter was the non-uniform surface charge distributions that could drive individual fibrils (or segments of long fibrils) to behave quite differently from the average behavior. This non-uniformity shows up in molecular-level failures along the inter-fibril surfaces which trigger local disintegration processes to begin. Thus, the non-uniformity underlies the wide fibril size distributions as well.

The charge of the surface carboxylate groups was screened by the moving counter-ions. Thus, the electrostatic forces in the functionalized system were not as large as the total charge of the fibril surfaces due to charged groups would have suggested. This screening has been assumed in previous continuous models (Fall et al. 2011; Fukuzumi et al. 2014) and is expected to take place also in real experimental systems. In the previous DLVO models, the diameter of the cylindrical fibrils was not clearly larger than their separation so that the used equations were not strictly valid. This uncertainty was removed in our atomistic molecular dynamics simulations. The obtained repulsive PMF level 10–20 kJ/mol (4–8 $k_B T$) at 1 nm fibril surface separation with 250 mM salt concentration was obtained at similar 200 mM bulk salt concentration in the DLVO model of Fukuzumi et al. (2014). However, the repulsive interaction extended to slightly shorter distances in the molecular dynamics simulations than for the DLVO model.

Although a real-life experiment of a similar system comprising two small fibrils immersed in water would be extremely difficult or even impossible to perform, these findings can be linked to larger scale experimental observations. The type of simulations carried out here could support the selection of chemical modification methods to be developed for better dispersion of the fibrils. The effect of degree of substitution on the interactions and properties of

functionalized fibrils could also be studied. In our simulations for two parallel nanofibrils, the separation of the average PMF curves reflected the experimentally measured changes in disintegration energy of modified cellulose fibrils in the Ystral Z 80-3 dispersion unit. Moreover, the observed variation of fibril–fibril interaction at intermediate functionalization levels could explain the heterogeneity of the disintegrated fibril structure obtained with the homogenizer. As to aggregation behavior and rheology, the studied case with parallel fibrils reflects the upper boundary of the repulsive interaction.

The comparison between molecular dynamics and real-life aggregation experiments is not straightforward due to several reasons, e.g., the length of the fibrils is restricted, the rotations of the fibrils are limited and possible amorphous coverages are not treated in the simulations while the distribution of functional groups is not known from the experiments. One way to improve the comparison would be enlarging the model systems so that the fibrils would be free to rotate in all directions allowing perpendicular arrangements that minimize the repulsive energy (Fukuzumi et al. 2014). The size of the simulation domain should be increased also to avoid artefacts due to the use of periodic boundary conditions, as our results indicate that the contribution of the neighboring periodic cells can have a significant effect on the PMF curves. However, even though direct comparison may not yet be feasible, the simulations improve the qualitative understanding of the interactions between carboxylated cellulose nanofibrils.

Acknowledgments The authors would like to thank Prof. Hans Theliander for valuable discussions and SCA Hygiene Products Ab, the foundation “Södra Skogsägarnas stiftelse för forskning, utveckling och utbildning”, and VINNOVA for financial support at the Chalmers University of Technology, where part of the experiments were carried out. CSC IT Center for Science Ltd. is acknowledged for providing computational resources for the simulations. A part of the data used in this research is from the EU SUNPAP project that received funding from the European Community’s Seventh Framework Programme under Grant Agreement No. 228802.

References

- Andersson S, Serimaa R, Paakkari T, Saranpää P, Pesonen E (2003) Crystallinity of wood and the size of cellulose crystallites in Norway spruce (*Picea abies*). *J Wood Sci* 49(6):531–537
- Brodin FW, Sonavane Y, Sedin M (2013a) Displacement washing of TEMPO-oxidized softwood kraft pulp: effects of change in fiber properties. *Nord Pulp Pap Res J* 28:366–376
- Brodin FW, Sonavane Y, Theliander H (2013b) Preparation of absorbent foam based on softwood kraft pulp: advancing from gram to kilogram scale. *Bioresources* 8:2099–2117
- Bussi G, Davide D, Parrinello M (2007) Canonical sampling through velocity rescaling. *J Chem Phys* 126(1):014101
- Chinga-Carrasco G (2011) Cellulose fibers, nanofibrils and microfibrils: the morphological sequence of MFC components from a plant physiology and fiber technology point of view. *Nanoscale Res Lett* 6:417
- Ding S-Y, Zhao S, Zeng Y (2014) Size, shape, and arrangement of native cellulose fibrils in maize cell walls. *Cellulose* 21:863–871
- Eichhorn SJ, Davies GR (2006) Modelling the crystalline deformation of native and regenerated cellulose. *Cellulose* 13:291–307
- Essmann U, Perera L, Berkowitz ML, Darden T, Lee H, Pedersen LG (1995) A smooth particle mesh Ewald method. *J Chem Phys* 103(19):8577–8593
- Fall AB, Lindström SB, Sundman O, Ödberg L, Wågberg L (2011) Colloidal stability of aqueous nanofibrillated cellulose dispersions. *Langmuir* 27:11332–11338
- Fukuzumi H, Tanaka R, Saito T, Isogai A (2014) Dispersion stability and aggregation behavior of TEMPO-oxidized cellulose nanofibrils in water as a function of salt addition. *Cellulose* 21:1553–1559
- Henriksson M, Henriksson G, Berglund LA, Lindstrom T (2007) An environmentally friendly method for enzyme-assisted preparation for microfibrillated cellulose (MFC) nanofibers. *Eur Polym J* 43:3434–3441
- Herrick FW, Casebier RL, Hamilton JK, Sandberg KR (1983) Microfibrillated cellulose: morphology and accessibility. *J Appl Polym Sci: Appl Polym Symp* 37:797–813
- Hess B, Bekker H, Berendsen HJC, Fraaije JGEM (1997) LINCS: a linear constraint solver for molecular simulations. *J Comput Chem* 18(12):1463–1472
- Hub JS, de Groot BL, van der Spoel D (2010) g_wham—a free weighted histogram analysis implementation including robust error and autocorrelation estimates. *J Chem Theory Comput* 6(12):3713–3720
- Jorgensen WL, Maxwell DS, Tirado-Rives J (1996) Development and Testing of the OPLS All-Atom Force Field on Conformational Energetics and Properties of Organic Liquids. *J Am Chem Soc* 118(45):11225–11236
- Kästner J (2011) Umbrella sampling. *Wiley Interdiscip Rev Comput Mol Sci* 1(6):932–942
- Kumar S, Rosenberg JM, Bouzida D, Swendsen RH, Kollman PA (1992) The weighted histogram analysis method for free-energy calculations on biomolecules I. The Method. *J Comput Chem* 13(8):1011–1021
- Matthews JF, Skopec CE, Mason PE, Zuccato P, Torget RW, Sugiyama J, Himmel ME, Brady JW (2006) Computer simulation studies of microcrystalline cellulose I β . *Carbohydr Res* 341:138–152
- Matthews JF, Bergensträhle M, Beckham GT, Himmel ME, Nimlos MR, Brady JW, Crowley MF (2011) High-temperature behavior of cellulose I. *J Phys Chem B* 115:2155–2166

- Moon RJ, Martini A, Nairn J, Simonsen J, Youngblood J (2011) Cellulose nanomaterials review: structure, properties and nanocomposites. *Chem Soc Rev* 40:3941–3994
- Nishiyama Y, Langan P, Chanzy H (2002) Crystal structure and hydrogen-bonding system in cellulose I β from synchrotron X-ray and neutron fiber diffraction. *J Am Chem Soc* 124(31):9074–9082
- Nishiyama Y, Johnson GP, French AD, Forsyth VT, Langan P (2008) Neutron crystallography, molecular dynamics, and quantum mechanics studies of the nature of hydrogen bonding in cellulose I β . *Biomacromolecules* 9(11):3133–3140
- Oehme DP, Doblin MS, Wagner J, Bacic A, Downton T, Gidley MJ (2015) Gaining insight into cell wall cellulose microfibril organisation by simulating microfibril adsorption. *Cellulose* 22(6):3501–3520
- Orlowski A, Róg T, Paavilainen S, Manna M, Heiskanen I, Backfolk K, Timonen J, Vattulainen I (2015) How endoglucanase enzymes act on cellulose nanofibrils: role of amorphous regions revealed by atomistic simulations. *Cellulose* 22(5):2911–2925
- Pääkkö M, Ankerfors M, Kosonen H, Nykänen A, Ahola S, Österberg M, Ruokolainen J, Laine J, Larsson PT, Ikkala O, Lindström T (2007) Enzymatic hydrolysis combined with mechanical shearing and high-pressure homogenization for nanoscale cellulose fibrils and strong gels. *Biomacromolecules* 8:1934–1941
- Paavilainen S, Róg T, Vattulainen I (2011) Analysis of twisting of cellulose nanofibrils in atomistic molecular dynamics simulations. *J Phys Chem B* 115:3747–3755
- Paavilainen S, McWhirter JL, Róg T, Järvinen J, Vattulainen I, Ketoja JA (2012) Mechanical properties of cellulose nanofibrils determined through atomistic molecular dynamics simulations. *Nord Pulp Paper Res J* 27:282–286
- Paster M, Pellegrino JL, Carole TM (2003) Industrial bioproducts: today and tomorrow. Department of Energy, Washington D.C, U.S
- Postek MT, Moon RJ, Rudie AW, Bilodeau MA (2013) Production and applications of cellulose nanomaterials. Tappi Press, Peachtree Corners
- Pronk S, Páll S, Schulz R, Larsson P, Bjelkmar P, Apostolov R, Shirts MR et al (2013) GROMACS 4.5: a high-throughput and highly parallel open source molecular simulation toolkit. *Bioinformatics* 29(7):845–854
- Saito T, Isogai A (2004) TEMPO-mediated oxidation of native cellulose. The effect of oxidation conditions on chemical and crystal structures of the water insoluble fractions. *Biomacromolecules* 5:1983–1989
- Saito T, Isogai A (2005) Ion-exchange behavior of carboxylate groups in fibrous cellulose oxidized by the TEMPO-mediated system. *Carbohydr Polym* 61:183–190
- Saito T, Nishiyama Y, Putaux JL, Vignon M, Isogai A (2006) Homogeneous suspensions of individualized microfibrils from TEMPO-catalyzed oxidation of native cellulose. *Biomacromolecules* 7:1687–1691
- Saito T, Kimura S, Nishiyama Y, Isogai A (2007) Cellulose nanofibers prepared by TEMPO mediated oxidation of native cellulose. *Biomacromolecules* 8:2485–2491
- Saito T, Hirota M, Tamura N, Kimura S, Fukuzumi H, Heux L, Isogai A (2009) Individualization of nano-sized plant cellulose fibrils by direct surface carboxylation using TEMPO catalyst under neutral conditions. *Biomacromolecules* 10(7):1992–1996
- Schütz C, Agthe M, Fall AB, Gordeyeva K, Guccini V, Salajková M, Plivelic TS, Lagerwall JPF, Salazar-Alvarez G, Bergström L (2015) Rod packing in chiral nematic cellulose nanocrystal dispersions studied by small-angle X-ray scattering and laser diffraction. *Langmuir* 31:6507–6513
- Stoyanov SR, Lyubimova O, Gusarov S, Kovalenko A (2014) Computational modeling of the structure relaxation and dispersion thermodynamics of pristine and modified cellulose nanocrystals in solution. *Nord Pulp Pap Res J* 29:44–155
- Torrie GM, Valleau JP (1977) Nonphysical sampling distributions in Monte Carlo free-energy estimation: umbrella sampling. *J Comput Phys* 23(2):187–199
- Turbak AF, Snyder FW, Sandberg KR (1983) Microfibrillated cellulose: a new cellulose product: properties, uses, and commercial potential. *J Appl Polym Sci: Appl Polym Symp* 37:815–827
- Wågberg L, Decher G, Norgren M, Lindström T, Ankerfors M, Axnäs K (2008) The build-up of polyelectrolyte multilayers of microfibrillated cellulose and cationic polyelectrolytes. *Langmuir* 24:784–795
- Yui T, Hayashi S (2007) Molecular dynamics simulations of solvated crystal models of cellulose I(α) and III. *Biomacromolecules* 8(3):817–824
- Yui T, Nishimura S, Akiba S, Hayashi S (2006) Swelling behavior of the cellulose I β crystal models by molecular dynamics. *Carbohydr Res* 341(15):2521–2530
- Zhang Q, Bulone V, Ågren H, Tu Y (2011) A molecular dynamics study of the thermal response of crystalline cellulose I β . *Cellulose* 18:207–221